# Understanding the True Shape of Au-Catalyzed GaAs Nanowires

**ARTICLE** *in* NANO LETTERS · SEPTEMBER 2014

Impact Factor: 13.59 · DOI: 10.1021/nl5027937 · Source: PubMed



**6 AUTHORS**, INCLUDING:

Nian Jiang
Australian National University
**22** PUBLICATIONS **185** CITATIONS
SEE PROFILE

J. Wong-Leung
Australian National University
**133** PUBLICATIONS **2,128** CITATIONS
SEE PROFILE

Hannah Jane Joyce
University of Cambridge
**113** PUBLICATIONS **2,126** CITATIONS
SEE PROFILE

Chennupati Jagadish
Australian National University
**282** PUBLICATIONS **3,469** CITATIONS
SEE PROFILE

NANO LETTERS

Letter

pubs.acs.org/NanoLett

# Understanding the True Shape of Au-Catalyzed GaAs Nanowires

Nian Jiang,*[,†] Jennifer Wong-Leung,[†,‡] Hannah J. Joyce,[§] Qiang Gao,[†] Hark Hoe Tan,[†] and Chennupati Jagadish[†]

[†]Department of Electronic Materials Engineering, Research School of Physics and Engineering, and [‡]Centre of Advanced Microscopy, The Australian National University, Canberra, ACT 0200, Australia

[§]Department of Engineering, University of Cambridge, Cambridge CB3 0FA, United Kingdom

Supporting Information

**ABSTRACT:** With increasing interest in nanowire-based devices, a thorough understanding of the nanowire shape is required to gain tight control of the quality of nanowire heterostructures and improve the performance of related devices. We present a systematic study of the sidewalls of Au-catalyzed GaAs nanowires by investigating the faceting process from the beginning with vapor−liquid−solid (VLS) nucleation, followed by the simultaneous radial growth on the sidewalls, and to the end with sidewall transformation during annealing. The VLS nucleation interface of our GaAs nanowires is revealed by examining cross sections of the nanowire, where the nanowire exhibits a Reuleaux triangular shape with three curved surfaces along {112}A. These curved surfaces are not thermodynamically stable and adopt {112}A facets during radial growth. We observe clear differences in radial growth rate between the ⟨112⟩A and ⟨112⟩B directions with {112}B facets forming due to the slower radial growth rate along ⟨112⟩B directions. These sidewalls transform to {110} facets after high temperature (>500 °C) annealing. A nucleation model is proposed to explain the origin of the Reuleaux triangular shape of the nanowires, and the sidewall evolution is explained by surface kinetic and thermodynamic limitations.

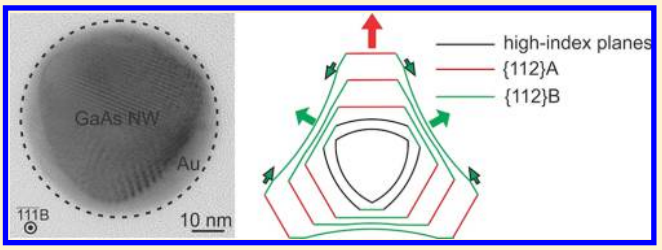


**KEYWORDS:** *GaAs, nanowires, vapor−liquid−solid nucleation, sidewall facets, cross sections*

Semiconductor nanowires have been a research focus in recent years due to their potential as nanobuilding blocks for future electronic and optoelectronic devices. Nanowire devices such as lasers,[1,2] LEDs,[2,3] solar cells,[4] terahertz detectors,[5] transistors,[6] and sensors[7] have already been demonstrated. Studies of planar structures show that the electronic properties (i.e., band structures,[8−10] mid-gap states, and Fermi level pinning,[11−13]) and chemical properties (i.e., surface energy[14] and passivation,[15] diffusion length[16]) of semiconductors vary along different crystal orientations. Accordingly, the performance of planar semiconductor devices is highly dependent on the orientation of the semiconductors surfaces, heterointerfaces, and homojunctions; this orientation effect is even more significant in nanowire-based devices because of their quasi-one-dimensional geometry and their high surface-to-volume-ratios. III−V nanowires most commonly grow in the [111]B direction and form with certain facets depending on the growth conditions and the underlying crystal structure of the nanowires.[17−19] Vapor−liquid−solid (VLS) nanowire growth has been extensively studied since its first demonstration.[20−22] Despite significant progress toward understanding nucleation processes, and the role of the triple-phase-line (TPL) and the pre-existing facets in nanowire growth,[23−26] the initial information on nanowire facets is still not well understood.

Furthermore, nanowire heterostructures underpins the majority of practical nanowire-based devices. The orientation and geometry of the nanowire facets will determine the quality and nature of heterointerfaces with nanowires.[27,28] Transformation of nanowire sidewall facets has been observed in core−shell structures.[29−31] It is reported that the sidewall facets of zinc blende (ZB) GaAs nanowires are of the {112} family.[23,32,33] These {112} facets, although thermodynamically unstable high-index planes,[34] form in nanowires due to the presence of the liquid nanoparticle and its role in VLS growth. In comparison, when a shell is grown around the GaAs nanowires, these facets transform mostly into {110} planes[35] or a mixture of {110} and {112} planes.[29,31] Facet transformation is an important issue because the facets of the GaAs core have been reported to impact the growth rate and composition uniformity of the shell during growth.[17,30] Despite the strong influence the nanowire core facet has on growth, the process of the facet transformation is far from well-understood.

In this work, we have systematically studied the facet formation and evolution in GaAs nanowires grown by the VLS technique. We show that pre-existing facets during VLS nucleation in MOCVD are not of the low-index planes but a

**Received:** July 22, 2014
**Revised:** September 10, 2014





dx.doi.org/10.1021/nl5027937 | *Nano Lett.* XXXX, XXX, XXX−XXX

series of high-index planes culminating into a Reuleaux triangular cross section. These high-index planes gradually evolved into the reported {112} facets[32] due to the simultaneous radial growth by the vapor−solid (VS) mechanism. The transformation of the sidewalls at high temperatures (typical for shell growth) into the {110} facets was also investigated. A nucleation theory is developed to explain the formation of the Reuleaux triangular cross section.

**Experiment.** Two sets of GaAs nanowires were grown on GaAs (111)B substrates by metal organic chemical vapor deposition (MOCVD) using Au particles as catalyst, with trimethylgallium (TMGa) and arsine ($AsH_3$) as the Ga and As source, respectively. Stacking fault-free ZB GaAs nanowires were grown by a two-temperature procedure with 1 min nucleation at 450 °C followed by 45 min growth at 375 °C.[36] Radial growth is minimized in this sample due to the low growth temperature so that the formation of facets due only to VLS growth can be studied.[36] The elimination of stacking faults also excludes the 180° rotation of polarity of the sidewalls caused by rotational twins about the growth direction. To investigate the effect of radial growth on the sidewall facets, another sample was grown at 450 °C for 46 min. The stacking fault density of this set of nanowires was very low (~1/$\mu$m) while radial growth was substantially enhanced.[36] Both sets of nanowires were grown with $AsH_3$/TMGa ratio of 46. To study facet evolution, the temperature was ramped to a range of 500−800 °C (which is the typical shell growth temperature in MOCVD[37,38]) after GaAs nanowire growth under $AsH_3$ ambient and maintained for 2 min before cooling down. This set of samples will be referred to as the annealed nanowires in this paper while the other two sets of nanowires will be referred to as as-grown nanowires.

Both scanning electron microscopy (SEM) and transmission electron microscopy (TEM) were used to study the sidewall facets of the nanowires. SEM gives the overall geometry of the nanowires while the orientations of the sidewall facets were determined by TEM. To identify the planes of the sidewall facets, cross-sectional TEM samples were prepared by microtome. Details are shown in the Supporting Information. The microtome lamellas were carefully picked up by using a copper grid with a lacey carbon film and loaded such that the $(\bar{1}\bar{1}\bar{1})$ plane (nominally (111)B) is facing the electron beam. Since {112} planes have different polarities, i.e. {112}A and {112}B, the polarity of the sidewalls was determined by careful analyses involving tilting the nanowires cross sections to different zone axes. Details are shown in Supporting Information Figure S3. This allowed us to identify facets along the entire nanowire length, including in the vicinity of the Au nanoparticle catalyst. This nanoparticle forms a Au−Ga alloy during the growth process but for simplicity will be referred as the "Au nanoparticle" here.

**Results and Discussion.** Figure 1a shows the SEM images of the two-temperature grown GaAs nanowires. The nanowires grew vertically on the substrate with a tapering parameter ((diameter at bottom−diameter at top)/length of nanowire) of <3 nm/$\mu$m. There is no resolvable faceting behavior on the nanowire directly beneath the Au particle. Indeed, clear faceting only starts to appear nearer to the substrate (Figure S2 in Supporting Information). A high-resolution TEM image of the tip of the nanowire, viewed along the ⟨110⟩ zone axis, is shown in Figure 1b. The nanowire shows a ZB structure free of stacking faults and a significant asymmetry when viewed along the ⟨110⟩ zone axis. The projections of {112}A and {112}B

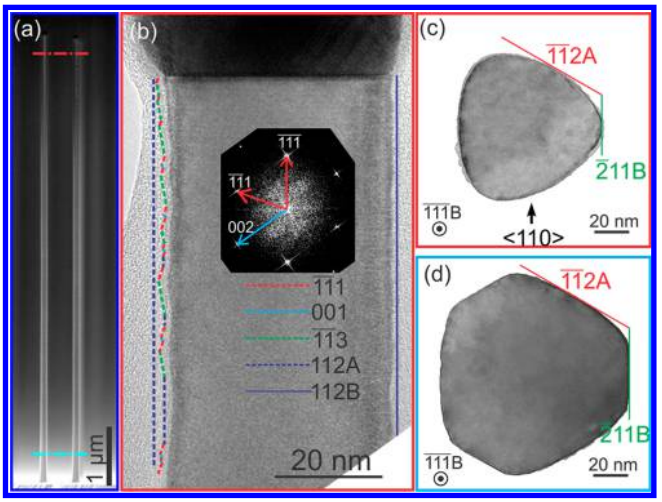


**Figure 1.** (a) SEM image of the two-temperature grown GaAs nanowires obtained at a tilt of 90°. The electron beam is parallel to ⟨110⟩. (b) High-resolution TEM images of the top of the nanowire in (a) with FFT pattern inserted. Indexed facets are marked with colored lines. (c, d) Cross-sectional TEM images from the top and the bottom of the nanowires as indicated by dotted lines in (a) with {112}A and {112}B planes indicated by red and green lines, respectively. The black arrow in (c) indicates the viewing direction for (b).

facets are indicated by the broken and solid blue lines on the left- and right-hand side of the nanowire, respectively. The {112}A side is composed of a series of extended sawtooth-like nanofacets including $(\bar{1}11)$ [nominally 111A], $(\bar{1}\bar{1}3)$ [A polar], (001), and $(\bar{1}\bar{1}2)$ [A polar] as indicated. In comparison, the {112}B side is smoother: the nanowire closely follows the projection of the {112}B facet, consisting only of $\{11\bar{1}\}$ and $\{00\bar{1}\}$ atomic steps.[32] It is interesting to note that the Au particle in Figure 1b shows asymmetry in the contact angle made with the nanowire, as will be explained below.

Cross-sectional samples from different part of nanowires were studied by TEM to investigate the sidewalls. Figure 1c,d shows the TEM images from the top and bottom of a nanowire (as indicated by red and blue dotted-lines in Figure 1a, respectively). Note that these two cross sections are not necessarily from the same nanowire. Surprisingly, instead of a hexagonal prism which is widely accepted as the shape of nanowires without any radial growth,[32] the cross section within 2 $\mu$m of the Au particle has the shape of a Reuleaux triangle consisting of three curved surfaces. With reference to the {112}A and {112}B planes indicated by the red and the green lines, respectively, it is clear that the curved surfaces are closer to {112}A planes (Figure 1c) while the corners point toward the ⟨112⟩B direction. Indeed, small {112}B facets were found where two curved surfaces meet. To distinguish the curved sidewall surfaces from the real {112}A planes, we shall hereafter refer to these curved surfaces as "{112}A curved" surfaces. In contrast, the cross-sectional TEM image in Figure 1d shows larger diameter at the bottom of the nanowire and indicates that some radial growth occurred on the sidewall facets, resulting in a truncated triangular cross section with well-defined {112}B facets while the {112}A curved surfaces remain curved but better defined compared to the top. The faceting is consistent with Figure S2 (Supporting Information) where the vertical contrast pointed out by the blue arrow is the intersection between the {112}B facets and the {112}A curved surfaces.


dx.doi.org/10.1021/nl5027937 | Nano Lett. XXXX, XXX, XXX−XXX

As reported by Joyce et al., radial growth is kinetically limited and suppressed at low growth temperature.[36] For the two-temperature grown nanowires, radial growth is so slow that the curved {112}A surfaces are maintained even at the bottom of the nanowire. To promote radial growth and study its influence on the faceting change, the growth temperature of nanowires was increased to 450 °C. Figure 2a shows SEM image of a GaAs nanowire grown at 450 °C. Significantly higher tapering is observed compared to the two-temperature grown nanowires. Faceting is clearly visible in the SEM images shown in Figure 2a. Cross-sectional images taken along the length of the nanowire are shown in Figure 2b–e from the top to the bottom with {112}A and {112}B as indicated by the green and red lines, respectively. The shape on the top of the nanowire is a Reuleaux triangle truncated by {112}B facets as shown in Figure 2b. During radial growth, the {112}A curved surfaces gradually flattened and changed to {112}A facets while the {112}B facets grew wider (Figure 2c). This indicates that the VLS-grown {112}A curved surfaces are not thermodynamically stable. Once {112}A facets are formed, the faster radial growth rate along the ⟨112⟩A direction compared to the ⟨112⟩B direction resulted in shrinkage of the {112}A facets and simultaneous formation of wider {112}B facets at the bottom of the nanowire (Figure 2d,e). It is interesting to note that {112}B sidewalls are flat initially (Figure 2b,c) and start to become slightly concave in the middle as they grow wider (Figure 2d,e). This concave shape is also observed in the SEM image (Figure S2 in Supporting Information).

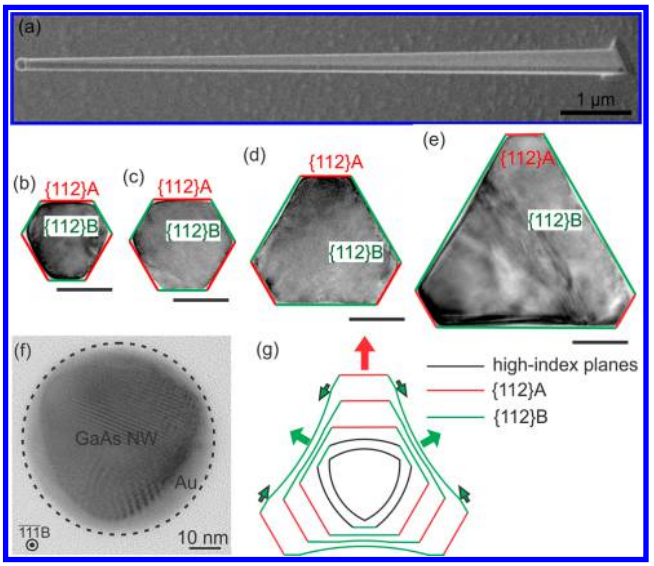


**Figure 2.** (a) SEM image of a GaAs nanowire grown at 450 °C taken at a 45° tilt. (b–e) Cross-sectional TEM images along the nanowire from the top to the bottom. {112}A and {112}B are represented by red and green solid lines, respectively. Scale bars are 50 nm. (f) Cross-sectional TEM image of a GaAs nanowire overlapping with a Au particle viewed along the $[\bar{1}\bar{1}\bar{1}]$ zone axis. (g) Schematic of sidewalls evolution during nanowire growth. The arrows indicate the growth directions.

To confirm the shape of the interface between the nanowire and the Au nanoparticle, cross-sectional samples with both Au nanoparticles and nanowires were prepared by microtoming with an approximate thickness of 50 nm. The radial growth of GaAs nanowire is negligible underneath the Au nanoparticle. Figure 2f shows the cross section of the Au particle and the nanowire underneath it imaged along the $[\bar{1}\bar{1}\bar{1}]$ zone axis. Indeed, the diameter of the VLS grown nanowire is smaller than the Au nanoparticle, consistent with the observation from SEM images (Figure S2 in Supporting Information). The Au nanoparticle exhibits a circular projection while the GaAs nanowire in the center has a Reuleaux triangular shape and shows a darker contrast. Moiré fringes arise in the overlap area of the Au nanoparticle and the nanowire due to the difference in lattice spacing between the Au particle and the nanowire. The different Moiré patterns indicate that the alloyed Au–Ga nanoparticle is multicrystalline in nature.

The nanoparticle–nanowire interface shows clear 3-fold symmetry with three long {112}A curved surfaces, as shown in Figures 1c and 2f. This noncircular interface shape distorts the nanoparticle, resulting in large contact angles meeting the {112}A curved surfaces and smaller contact angles meeting the {112}B corners. This asymmetry of nanoparticle contact angles is clearly observed in Figure 1b, in which a larger contact angle is observed adjacent to the left-hand {112}A facet and smaller contact angle observed adjacent to the right-hand {112}B facet.

The shape of the nanowire cross section from the 450 °C growth is consistent with the shape of the two-temperature grown nanowires. Figure 2g summarizes the facets evolution caused by radial growth. Starting from three {112}A curved surfaces, they grow flatter and finally become {112}A facets while the {112}B facets only develop from radial growth due to the relatively slow growth rate along the ⟨112⟩B directions. The concave shape of the {112}B facets also develops during radial growth as a result of the difference in growth rates between the ⟨112⟩A directions and ⟨112⟩B directions. The mechanism of formation of the concave shape of {112}B facets will be discussed later.

Figure 3 compares the {112}A curved surfaces and the concave {112}B sidewalls of the nanowires grown at 450 °C. The Reuleaux triangular shape on the top of the nanowire is shown in Figure 3a. The high-resolution TEM image of the {112}A curved surface (Figure 3b) shows a rounded surface. No obvious microsteps are observed. In contrast, high-resolution TEM images show that {112}B is faceted in the region close to the corner (Figure 3d) while a series of atomic steps can be seen near the center of the {112}B facets (Figure 3e), resulting in the concave appearance of this facet. The atomic structure of these curved surfaces indicates different mechanisms for their formation. The concave shape formed during radial growth and is related to atomic steps. On the other hand, the existence of the rounded morphology suggests the influence of the liquid nanoparticle catalyst on the nanowire growth, which will be discussed in detail later.

For typical nanowire core–shell heterostructures grown by the VLS mechanism by MOCVD, shell growth is typically carried out at a higher temperature than that of the core to overcome the kinetic barrier for VS growth.[39] The high growth temperature may also provide the energy for the nanowire sidewalls to adopt the lowest surface energy facets. To study the effect of temperature on the sidewalls, we annealed GaAs nanowires grown with the two-temperature growth method at 750 °C (which is a typical AlGaAs shell growth temperature) for 2 min under $AsH_3$ ambient.[35] Figure 4 shows the facets of the annealed nanowire. The length of nanowires remains the same (Figure 4a) during annealing while the tapering parameter is reduced to less than 1.5 nm/μm. The reduction of the tapering parameter is most likely a result of atomic migration on the side facets or surface evaporation. This reduction in


dx.doi.org/10.1021/nl5027937 | Nano Lett. XXXX, XXX, XXX–XXX

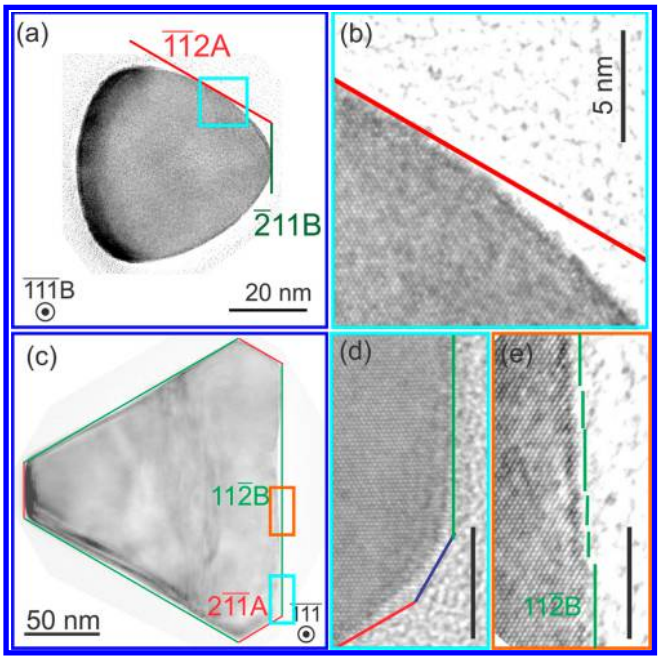


**Figure 3.** Comparison of the curved sidewalls between from the top (a, b) and the bottom (c–e) of the nanowires. (a) TEM image of a Reuleaux triangular cross section. An atomic resolution TEM image from the area highlighted by the blue box is shown in (b). The atomic resolution TEM images from the highlighted area in the blue and orange boxes in (c) are shown in (d) and (e), respectively. Scale bars in (d, e) are 5 nm. {112}A, {112}B, and {110} facets are indicated by red, green, and blue lines, respectively.

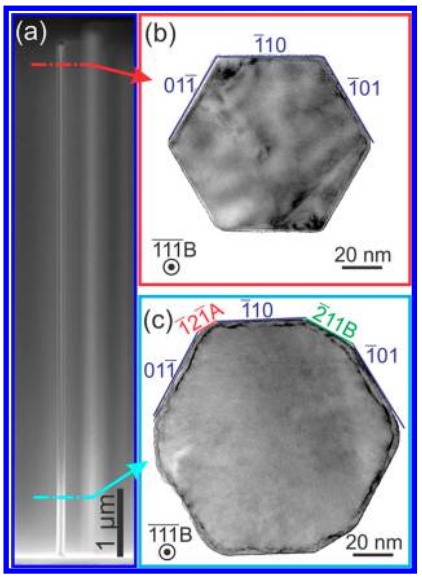


**Figure 4.** (a) SEM image, viewed at a tilt of 90°, of the two-temperature grown GaAs nanowires after 2 min annealing at 750 °C. The electron beam is parallel to ⟨110⟩. Red and blue dotted lines in (a) show the place where the cross sections in (b) and (c) were taken, respectively. {112}A, {112}B, and {110} planes are indicated in the TEM images.

tapering parameter became more obvious with longer annealing time, indicating obvious surface evaporation as shown in Figure S6 of the Supporting Information. Cross-sectional samples of the annealed nanowires were studied by TEM to identify the facets. In contrast to the as-grown nanowire, Figure 4b shows that the top of the annealed nanowire has six main {110} facets, while at the bottom the {110} facets are truncated by smaller {112} families as shown in Figure 4c. The {112} facets show a 3-fold symmetry with {112}A facets as the smallest section (marked by red lines). Details of the facets change along the nanowire are shown in Figure S2 of the Supporting Information.

Facet transformation from {112} to {110} requires significant surface diffusion of atoms. The speed of this facet transformation is influenced by the kinetic energy barrier of surface diffusion, the difference in surface energies (driving force) between the original facet and the newly formed facets, the material volume involved, and the migration distance. The material volume involved and the migration distances for different cross-sectional shapes were calculated (Figure S4 in Supporting Information). Since the sidewalls of annealed nanowires have both {110} and {112} facets, the facet transformation speed can be indicated by the remaining size of the {112} facets. Smaller {112} facets indicate faster transformation. The width of {112} facets is negligible at the top of nanowires and increases toward the bottom, as shown in Figure 4. This occurs despite the longer migration distance for the Reuleaux triangular shape present at the top of the nanowires. It is also interesting to note that for the annealed nanowires the sidewalls have fully transformed into {110} facets at the top of the nanowires even for those catalyzed by 150 nm Au particles (Figure S5d in Supporting Information) while {112} facets still remain at the bottom of nanowires catalyzed by 100 nm particles where the diameter is less than 130 nm (Figure 4c). These observations imply that the original surface morphologies play a determining role in facet transformation. This occurs despite the longer migration distance for the nanowire with larger diameters. These observations suggest that the original shape and orientation of the facets determine the speed of transformation more significantly than the migration distance. The rounded surfaces (top of nanowires) transformed to straight {110} facets which have the lowest surface energy configurations.[14] In contrast, the established faceted surfaces that evolved through radial growth (bottom of nanowires), e.g. {112} surfaces with a lower surface energy configuration than the curved {112}A surfaces, evolve more slowly. The fact that the {112}A facets are always narrower than {112}B facets at a fixed height indicates that the surface energy of the {112}A facets is higher than that of the {112}B facets, which is consistent with the surface energy diagram in Figure S8 (Supporting Information) under an As-rich regime.

To understand the sidewalls behavior of the nanowires, a model is first devised to explain the formation of the Reuleaux triangle with three {112}A curved surfaces. Typically, the nucleation theory for VLS growth assumes the nanowire adopts circular[33] or hexagonal cross sections under the Au particle.[21,23,40,41] The fact that we observe a Reuleaux triangle shape here warrants some discussion. Since no stacking faults are involved in this growth (the two-temperature method), our model takes into account (a) the surface of the Au particle and (b) the facets in the vicinity of the nanowire growth front and the Au–nanowire interface. Prior to nanowire growth, the Au particle is alloyed with Ga and forms a Au–Ga droplet. On an ideal isotropic surface, the droplet would adopt the shape of a truncated sphere with a circular droplet–nanowire interface to minimize the surface energy. Figure 5a shows a generic schematic of the nanowire growth front. Thus, the effective


dx.doi.org/10.1021/nl5027937 | Nano Lett. XXXX, XXX, XXX–XXX

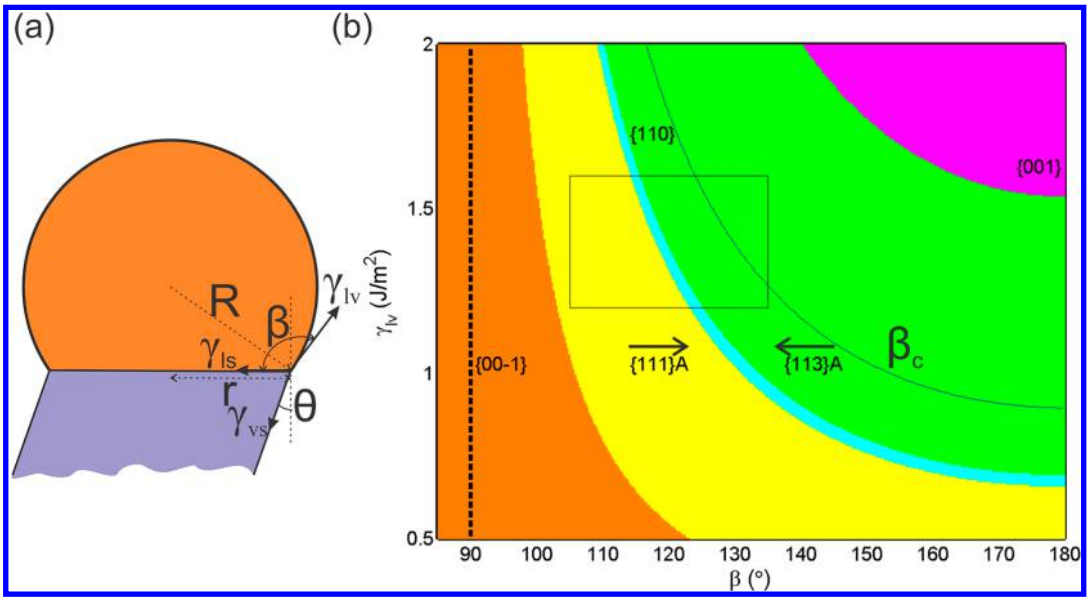


**Figure 5.** (a) Schematic of the VLS growth front with the parameters indicated. (b) Diagram of the preferred facets as a function of $\gamma_{lv}$ and $\beta$, assuming single layer growth at the liquid−solid interface. The rectangle represents the most likely parameter ranges based on our experimental work. The solid line indicates the optimum $\beta$ ($\beta_c$) with the lowest $E_{eff}$ before the nanowire growth initiated. Black arrows indicate the change direction of $\beta$ during growth. $\beta$ decreases each time a {113}A facet forms and increases each time a {111}A facet forms.

surface energy ($E_{eff}$) consists of two parts: the surface energy of the droplet and the droplet−nanowire interface energy:

$$E_{eff} = \gamma_{lv}(2\pi R^2)(1 - \cos\beta) + \gamma_{sl}\{\pi r^2\} \quad (1)$$

where

$$R = \left\{\frac{3V}{\pi}\frac{1}{\cos^3\beta - 3\cos\beta + 2}\right\}^{1/3} \quad (2)$$

$$r = R\sin\beta \quad (3)$$

Here, $\beta$ is the wetting angle, $r$ is the radius of the droplet−nanowire interface, and $R$ is the radius of the truncated droplet sphere, as shown in the schematic in Figure 5a. $\gamma_{lv}$ and $\gamma_{sl}$ represent the energies of the droplet−vapor surface and droplet−nanowire interface, respectively. $V$ is the volume of the droplet and is treated as a unit since it only changes the absolute value of $E_{eff}$. The value of $\gamma_{lv}$ is dependent on the Ga concentration in the droplet.[42] For Ga-related nanowire growth by MOCVD, $\gamma_{lv}$ is estimated in a range of 1.2−1.6 J/m$^2$.[42] According to eq 1, the optimum $\beta$ ($\beta_c$) with the lowest $E_{eff}$ can be calculated as a function of $\gamma_{lv}$, as detailed in the Supporting Information.

To form a single crystalline layer at the nanoparticle−nanowire interface, a change of the effective surface energy ($\Gamma_i$) is involved:[21]

$$\Gamma_i = \frac{\gamma_i}{\cos\theta_i} + \gamma_{ls}\tan\theta_i - \gamma_{vl}\frac{\sin(\beta - \theta_i)}{\cos\theta_i} \quad (4)$$

where $\theta_i$ is the inclination angle of the sidewall facet of the crystalline layer relative to the vertical plane and $\gamma_i$ is the surface energy of this external nucleus facet. The derivation of the formula is given in the Supporting Information and follows nucleation theory presented in recent publications.[23,25,26,34] The observed faceting behavior in Figure 1b shows the possible formation of various nucleus facets, such as the {100}, {111}, {112}, and {113} families. Apart from these facets, the {110} family is also among the most reported sidewall facets.[35,43] It is well-known that the {112} facets are not atomically flat but contain both {111} and {100} sidewall nanofacets.[32] Thus, for a single layer growth model, the main sidewall families considered are {100}, {111}, {113}, and {110} families. Based on this calculation, the facets with the lowest $\Gamma$ are plotted as a function of $\gamma_{lv}$ and $\beta$ in Figure 5b. The critical wetting angle, $\beta_c$, that minimizes $E_{eff}$ for a given $\gamma_{lv}$ before nanowire growth is initiated, was calculated according to eqs 1−3 and also plotted on top of this facet preference diagram. The fact that $\beta_c$ is located in the {113}A region with respect to the range of $\gamma_{lv}$ indicates that {113}A would be the most energetically preferred nucleus facets.

However, rather than a circular nanoparticle−nanowire interface, the interface instead exhibits 3-fold symmetry about the $[\bar{1}11]$ direction and takes the shape of a Reuleaux triangle. The noncircular interface shape is associated with a range of wetting angles $\beta$ at the TPL as observed in Figure 1b and discussed earlier. Based on the measurements of $\beta$ from TEM images and the approximation of $\gamma_{lv}$ in ref 42, a rectangle is added in Figure 5b. The width of the rectangle represents the range of $\beta$, and the height represents the range of $\gamma_{lv}$. The rectangle covers a region consistent with {111}A, {110}, and {113}A regimes as the most stable sidewall facets for minimizing the change of effective surface energy $\Gamma_i$. According to Breuer et al.,[34] $\beta$ only changes rapidly close to the corners of the nucleation prism. In our case, these are the corners of the Reuleaux triangle. As a result, {113}A would be favored along most of the TPL.

In our model, we only considered contact angles $\beta$ greater than 90° for two reasons. First, our analysis of numerous unannealed nanowires postgrowth did not reveal any contact angles less than 90°. Postgrowth measurements generally underestimate both the volume and the contact angles of the nanoparticle during growth because the nanoparticle loses Ga atoms during postgrowth cooling, to reduce the droplet volume and contact angles. Our postgrowth evidence indicates that the contact angles are greater than 90° throughout growth. Second,


dx.doi.org/10.1021/nl5027937 | Nano Lett. XXXX, XXX, XXX−XXX

solution of the Young equation indicates that VLS growth at the nanowire tip requires that the contact angle is greater than 90°, as shown by Dubrovskii.[21]

To maintain stable $[\bar{1}\bar{1}\bar{1}]$ oriented nanowire growth, $\theta$ has to be 0° at the macro scale. The formation of {113}A facets, for which $\theta > 0$, increase the droplet−nanowire interface area, in effect pulling the droplet taut and decreasing the wetting angle $\beta$. This pushes the system away from its minimum-energy state. As $\beta$ decreases, the system moves into a different region of the facet preference diagram (Figure 5b). Thus, the system will eventually adopt {110} or {111}A facets. Nonetheless, {110} facets cannot lower $E_{\text{eff}}$ as $\theta = 0$ in this case, and the {110} facets are only preferred over a narrow range of $\beta$. Thus, it is more likely for the system to adopt {111}A facets. This is consistent with the observation of alternating {111}A and {113}A microfacets in Figure 1b. {111}A planes have a negative $\theta$ (inclining in) while {113}A planes have a positive $\theta$ (inclining out). Thus, the alternate growth of {111}A and {113}A facets compensates for the change at the droplet−nanowire interface caused by $\theta$ and results in {112}A surface at the macroscale, as shown in Figure S11b of the Supporting Information. The shape of the {112}A curved surface is inherited from the shape of TPL because the droplet tends to form a truncated sphere shape to reduce the surface energy. As a result, the Reuleaux triangle with {112}A curved surfaces is observed.

The facet preference diagram of Figure 5b indicates the stability of the nuclei with {111}A and {113}A facets, resulting in overall {112}A facets. We now consider the processes occurring at the {112}B facets which exist opposite each {112}A facet. Figure 5b indicates that nuclei with {112}B facets are less energetically favorable, even considering the possibilities of {111}B, {113}B, and {001} subfacets. Furthermore, our TEM investigations have shown that at the nanoparticle−nanowire interface {112}B facets are considerably narrower than the {112}A curved facets. We therefore deduce that nucleation is more probable at {112}A facets than at {112}B facets. Further discussion of the process occurring at the {112}B sidewall facets is shown in the Supporting Information.

The formation of the {112}A Reuleaux triangle during VLS growth results from the minimization of the system energy of the growth front, including the Au particle, nucleus, and the interface. However, the curved {112}A surfaces constitute thermodynamically unstable high-index planes. These high-index planes will adopt low-index planes to lower the total surface energy through radial growth or surface atom migration after VLS nucleation. We believe there is a kinetic energy barrier/activation energy for the stabilization of the relevant low-index surfaces. This kinetic energy barrier can be overcome by thermal energy. The fact that the radial growth rate increases rapidly with growth temperature indicates that the kinetic energy barrier controls the radial growth.[44] Radial growth may be facilitated at the curved {112}A surfaces by the presence of step edges. The differences in growth rates on different planes will determine the final equilibrium shape of the nanowire sidewalls. Consequently, {112}A curved surfaces will flatten into the proper {112}A facets. Because the radial growth along the ⟨112⟩B is slower compared to the ⟨112⟩A directions, the {112}B facets become wider compared to the {112}A facets and eventually adopt a concave shape as can be seen close to the bottom of nanowire (Figure 2). Indeed, the microstep structures shown in the center of {112}B-concaved sidewalls (Figure 3e) provide evidence for the slower growth on {112}B facets as the limiting factor for the concave nature of the facets. Under the annealing conditions used, the kinetic energy barrier is overcome by the thermal energy. Thus, the sidewalls are transformed into {110} facets which have the lowest surface energy. This is also consistent with the fact that facet transformation rate is controlled by the surface energy differences.

Based on the results in this work, the facets of Au-catalyzed nanowires tend to form a Reuleaux triangle as a result of the liquid droplet and the 3-fold symmetry of the substrate about the growth direction. The facets of the VLS nuclei are determined by the surface energies ($\gamma_{\text{vs}}$) which are a function of the chemical potential difference between As vapor and As bulk ($\Delta\mu$) (see Supporting Information). We add that $\Delta\mu$ is a function of the type of catalyst, the sources involved in nanowire growth, the partial pressure of the species, and growth temperature. For instance, ZB nanowires grown by Ga-assisted molecular beam epitaxy (MBE) have {110} facets,[45,46] unlike the Au-assisted nanowires in our present study.

The Reuleaux-shaped nanowires have not previously been reported, and there are two possible reasons. First, there has been no detailed study on the actual cross section of the shape of the nucleation interface. Most of the facet determinations of the nanowires were carried out by viewing from the top of the nanowires,[32,47] where the view of the nanowires just below the catalyst is blocked since the catalyst is typically larger than the nucleation interface.[21] A few studies of the nanowires morphology have been carried out by TEM tomography.[33,48,49] However, the complexity involved in the reconstruction process of tomography makes it rather challenging to obtain atomic resolution to observe the Reuleaux triangular shape.[48] Second, the Reuleaux polygon is very difficult to observe in nanowires grown at high temperature where the VLS grown facets can be obsecured due to fast simultaneous VS growth and/or surface atom migration. Hence, properly developed facets are commonly reported in both MOCVD and MBE growth.[50,51] We believe in our as-grown nanowires we manage to capture a unique metastable state because of the slow radial growth rate and minimal surface atom migration at our chosen low growth temperatures.

In this work, we have systematically studied the sidewalls of VLS-grown nanowires and the effect of simultaneous radial growth on the sidewalls via the VS mechanism. A Reuleaux triangle with three {112}A curved surfaces is revealed as the actual shape of the nanowire at the growth interface. This Reuleaux triangle is thermodynamically unstable and can change to well-defined {112} facets due to polarity-driven VS growth that occurs simultaneously or can adopt {110} facets as a result of surface atom migration once sufficient energy is provided to overcome the kinetic energy barrier. A model based on the VLS nucleation theory was used to explain the unusual {112}A curved surfaces, and the sidewall behavior of nanowires was explained by the surface kinetics and thermodynamics. This model complements the VLS growth theory and questions the assumption in many studies that the nanowire top has a hexagonal shape.[23,24,40] The study of how the facets transform at high temperatures provides a further insight into the understanding of how the facets of subsequent shell growth occur.


dx.doi.org/10.1021/nl5027937 | Nano Lett. XXXX, XXX, XXX−XXX

## ■ ASSOCIATED CONTENT

### Supporting Information

Studies of facet behaviors by SEM, microtome processing and polarity determination, surface atom migration and evaporation during high temperature annealing, and the details of nucleation theory. This material is available free of charge via the Internet at http://pubs.acs.org.

## ■ AUTHOR INFORMATION


### Corresponding Author

*E-mail: jenny.nainjiang@anu.edu.au (N.J.).


### Notes

The authors declare no competing financial interest.

## ■ ACKNOWLEDGMENTS

The Australian Research Council (ARC) is acknowledged for its financial support, and the authors acknowledge the use of facilities in the Centre of Advanced Microscopy (AMMRF node), the ACT node of the Australian National Fabrication Facility. H.J.J. acknowledges the Royal Commission for the Exhibition of 1851 for her research fellowship.

## ■ ABBREVIATIONS

MOCVD, metal organic chemical vapor deposition; TMGa, trimethylgallium; TMAl, trimethylaluminum; $AsH_3$, arsine; VLS, vapor−liquid−solid; VS, vapor−solid; ZB, zinc blende; TPL, triple-phase-line; SEM, scanning electron microscopy; TEM, transmission electron microscopy.

## ■ REFERENCES


(1) Saxena, D.; Mokkapati, S.; Parkinson, P.; Jiang, N.; Gao, Q.; Tan, H. H.; Jagadish, C. *Nat. Photonics* **2013**, *7*, 963.
(2) Huang, M. H.; Mao, S.; Feick, H.; Yan, H.; Wu, Y.; Kind, H.; Weber, E.; Russo, R.; Yang, P. *Science* **2001**, *292*, 1897.
(3) Tomioka, K.; Motohisa, J.; Hara, S.; Hiruma, K.; Fukui, T. *Nano Lett.* **2010**, *10*, 1639.
(4) Krogstrup, P.; Jørgensen, H. I.; Heiss, M.; Demichel, O.; Holm, J. V.; Aagesen, M.; Nygard, J.; i Morral, A. F. *Nat. Photonics* **2013**, *7*, 306−310.
(5) Vitiello, M. S.; Coquillat, D.; Viti, L.; Ercolani, D.; Teppe, F.; Pitanti, A.; Beltram, F.; Sorba, L.; Knap, W.; Tredicucci, A. *Nano Lett.* **2012**, *12*, 96.
(6) Patolsky, F.; Timko, B. P.; Yu, G.; Fang, Y.; Greytak, A. B.; Zheng, G.; Lieber, C. M. *Science* **2006**, *313*, 1100.
(7) Shao, M. W.; Shan, Y. Y.; Wong, N. B.; Lee, S. T. *Adv. Funct. Mater.* **2005**, *15*, 1478.
(8) Qian, G.-X.; Martin, R. M.; Chadi, D. *Phys. Rev. B* **1988**, *37*, 1303.
(9) Mazur, A.; Pollmann, J. *Phys. Rev. B* **1984**, *30*, 2084.
(10) Chadi, D. J. *J. Vac. Sci. Technol., B* **1985**, *3*, 1167.
(11) Spicer, W. E.; Pianetta, P.; Lindau, I.; Chye, P. W. *J. Vac. Sci. Technol.* **1977**, *14*, 885.
(12) Offsey, S. D.; Woodall, J. M.; Warren, A. C.; Kirchner, P. D.; Chappell, T. I.; Pettit, G. D. *Appl. Phys. Lett.* **1986**, *48*, 475.
(13) Katnani, A.; Chadi, D. *Phys. Rev. B* **1985**, *31*, 2554.
(14) Moll, N.; Kley, A.; Pehlke, E.; Scheffler, M. *Phys. Rev. B* **1996**, *54*, 8844.
(15) Miller, E. A.; Richmond, G. L. *J. Phys. Chem. B* **1997**, *101*, 2669.
(16) Koshiba, S.; Nakamura, Y.; Tsuchiya, M.; Noge, H.; Kano, H.; Nagamune, Y.; Noda, T.; Sakaki, H. *J. Appl. Phys.* **1994**, *76*, 4138.
(17) Zheng, C.; Wong-Leung, J.; Gao, Q.; Tan, H. H.; Jagadish, C.; Etheridge, J. *Nano Lett.* **2013**, *13*, 3742.
(18) Ansbæk, T.; Semenova, E. S.; Yvind, K.; Hansen, O. *J. Vac. Sci. Technol., B* **2013**, *31*, 011209.
(19) Cich, M. J.; Johnson, J. A.; Peake, G. M.; Spahn, O. B. *Appl. Phys. Lett.* **2003**, *82*, 651.
(20) Wagner, R. S.; Ellis, W. C. *Appl. Phys. Lett.* **1964**, *4*, 89.
(21) Dubrovskii, V. G. *Technol. Phys. Lett.* **2011**, *37*, 53.
(22) Krogstrup, P.; Jørgensen, H. I.; Johnson, E.; Madsen, M. H.; Sørensen, C. B.; Morral, A. F. i.; Aagesen, M.; Nygård, J.; Glas, F. *J. Phys. D: Appl. Phys.* **2013**, *46*, 313001.
(23) Joyce, H. J.; Wong-Leung, J.; Gao, Q.; Tan, H. H.; Jagadish, C. *Nano Lett.* **2010**, *10*, 908.
(24) Ross, F. M.; Tersoff, J.; Reuter, M. C. *Phys. Rev. Lett.* **2005**, *95*, 146104.
(25) Glas, F.; Harmand, J.-C.; Patriarche, G. *Phys. Rev. Lett.* **2007**, *99*, 146101.
(26) Johansson, J.; Karlsson, L. S.; Svensson, C. P. T.; Mårtensson, T.; Wacaser, B. A.; Deppert, K.; Samuelson, L.; Seifert, W. *Nat. Mater.* **2006**, *5*, 574.
(27) Paladugu, M.; Zou, J.; Guo, Y.-N.; Zhang, X.; Joyce, H. J.; Gao, Q.; Tan, H. H.; Jagadish, C.; Kim, Y. *Angew. Chem., Int. Ed.* **2009**, *48*, 780.
(28) Paladugu, M.; Zou, J.; Guo, Y.-N.; Zhang, X.; Joyce, H. J.; Gao, Q.; Tan, H. H.; Jagadish, C.; Kim, Y. *Appl. Phys. Lett.* **2008**, *93*, 201908.
(29) Skold, N.; Wagner, J. B.; Karlsson, G.; Hernan, T.; Seifert, W.; Pistol, M. E.; Samuelson, L. *Nano Lett.* **2006**, *6*, 2743.
(30) Wagner, J. B.; Skold, N.; Wallenberg, L. R.; Samuelson, L. *J. Cryst. Growth* **2010**, *312*, 1755.
(31) Tambe, M. J.; Allard, L. F.; Gradečak, S. *J. Phys.: Conf. Ser.* **2010**, *209*, 012033.
(32) Zou, J.; Paladugu, M.; Wang, H.; Auchterlonie, G. J.; Guo, Y. N.; Kim, Y.; Gao, Q.; Joyce, H. J.; Tan, H. H.; Jagadish, C. *Small* **2007**, *3*, 389.
(33) Verheijen, M. A.; Algra, R. E.; Borgström, M. T.; Immink, G.; Sourty, E.; van Enckevort, W. J. P.; Vlieg, E.; Bakkers, E. P. A. M. *Nano Lett.* **2007**, *7*, 3051.
(34) Breuer, S.; Feiner, L.-F.; Geelhaar, L. *Cryst. Growth Des.* **2013**, *13*, 2749.
(35) Jiang, N.; Gao, Q.; Parkinson, P.; Wong-Leung, J.; Mokkapati, S.; Breuer, S.; Tan, H. H.; Zheng, C. L.; Etheridge, J.; Jagadish, C. *Nano Lett.* **2013**, *13*, 5135.
(36) Joyce, H. J.; Gao, Q.; Tan, H. H.; Jagadish, C.; Kim, Y.; Zhang, X.; Guo, Y. N.; Zou, J. *Nano Lett.* **2007**, *7*, 921.
(37) Jiang, N.; Parkinson, P.; Gao, Q.; Breuer, S.; Tan, H. H.; Wong-Leung, J.; Jagadish, C. *Appl. Phys. Lett.* **2012**, *101*, 023111.
(38) Skold, N.; Karlsson, L. S.; Larsson, M. W.; Pistol, M. E.; Seifert, W.; Tragardh, J.; Samuelson, L. *Nano Lett.* **2005**, *5*, 1943.
(39) Stringfellow, G. B. *Organometallic Vapor-Phase Epitaxy: Theory and Practice*; Academic Press, Inc.: New York, 1989.
(40) Krogstrup, P.; Curiotto, S.; Johnson, E.; Aagesen, M.; Nygård, J.; Chatain, D. *Phys. Rev. Lett.* **2011**, *106*, 125505.
(41) Dubrovskii, V. G.; Sibirev, N. V. *Phys. Rev. E* **2004**, *70*, 031604.
(42) Algra, R. E.; Verheijen, M. A.; Feiner, L.-F.; Immink, G. G. W.; Enckevort, W. J. P. v.; Vlieg, E.; Bakkers, E. P. A. M. *Nano Lett.* **2011**, *11*, 1259.
(43) Hjort, M.; Lehmann, S.; Knutsson, J.; Timm, R.; Jacobsson, D.; Lundgren, E.; Dick, K. A.; Mikkelsen, A. *Nano Lett.* **2013**, *13*, 4492.
(44) Joyce, H. J.; Qiang, G.; Wong-Leung, J.; Kim, Y.; Tan, H. H.; Jagadish, C. *IEEE J. Sel. Top. Quantum Electron.* **2011**, *17*, 766.
(45) Fontcuberta i Morral, A.; Spirkoska, D.; Arbiol, J.; Heigoldt, M.; Morante, J. R.; Abstreiter, G. *Small* **2008**, *4*, 899.
(46) Rieger, T.; Heiderich, S.; Lenk, S.; Lepsa, M. I.; Grützmacher, D. *J. Cryst. Growth* **2012**, *353*, 39.
(47) Cirlin, G. E.; Dubrovskii, V. G.; Samsonenko, Y. B.; Bouravleuv, A. D.; Durose, K.; Proskuryakov, Y. Y.; Mendes, B.; Bowen, L.; Kaliteevski, M. A.; Abram, R. A.; Zeze, D. *Phys. Rev. B* **2010**, *82*, 035302.
(48) Alpers, A.; Gardner, R. J.; König, S.; Pennington, R. S.; Boothroyd, C. B.; Houben, L.; Dunin-Borkowski, R. E.; Joost Batenburg, K. *Ultramicroscopy* **2013**, *128*, 42.
(49) Wu, J.; Padalkar, S.; Xie, S.; Hemesath, E. R.; Cheng, J.; Liu, G.; Yan, A.; Connell, J. G.; Nakazawa, E.; Zhang, X.; Lauhon, L. J.; Dravid, V. P. *J. Phys. Chem. C* **2012**, *117*, 1059.

(50) Lehmann, S.; Wallentin, J.; Jacobsson, D.; Deppert, K.; Dick, K. A. *Nano Lett.* **2013**, *13*, 4099.
(51) Conesa-Boj, S.; Kriegner, D.; Han, X.-L.; Plissard, S.; Wallart, X.; Stangl, J.; Fontcuberta i Morral, A.; Caroff, P. *Nano Lett.* **2014**, *14*, 326.


dx.doi.org/10.1021/nl5027937 | *Nano Lett.* XXXX, XXX, XXX−XXX